

Sense-and-Predict: Harnessing Spatial Interference Correlation for Opportunistic Access in Cognitive Radio Networks

Jeemin Kim, Seung-Woo Ko, Han Cha, Seunghwan Kim, and Seong-Lyun Kim

Abstract

Cognitive radio (CR) is a key enabler realizing 5G networks to achieve higher spectral efficiency by allowing spectrum sharing between different wireless networks. It is important to explore whether spectrum access opportunities are available, but conventional CR based on *transmitter* (TX) sensing cannot be used to this end because the paired *receivers* (RXs) may experience different levels of interference, according to the extent of their separation and blockages. To address this problem, this paper proposes a novel form of *medium access control* (MAC) termed *sense-and-predict* (SaP), whereby each secondary TX predicts the interference level at the RX based on the sensed interference at the TX; this can be quantified in terms of a spatial interference correlation between the two locations. Using stochastic geometry, the spatial interference correlation can be expressed in the form of a conditional coverage probability, such that *the signal-to-interference ratio* (SIR) at the RX is no less than a predetermined threshold dictated by the sensed interference at the TX, defined as an *opportunistic probability* (OP). The secondary TX randomly accesses the spectrum with probability OP. We optimize the SaP framework to maximize the *area spectral efficiencies* (ASEs) of secondary networks while guaranteeing the service quality of the primary networks. Testbed experiments using USRP and MATLAB simulations show that SaP affords higher ASEs compared with CR without prediction.

I. INTRODUCTION

Spectrum has become the most important and scarce resource during the period in which wireless communications have expanded enormously. Many efforts have been made to extend the range of the usable spectrum even when it is already used by others; the research field is termed *cognitive radio* (CR) [1]. By allowing spectrum-sharing among different wireless networks, CR is

J. Kim, H. Cha, S. Kim and S.-L. Kim are with the School of Electrical and Electronic Engineering, Yonsei University, Seoul, Korea (email: {jmkim, chan, shkim}@ramo.yonsei.ac.kr, slkim@yonsei.ac.kr), S.-W. Ko is with the Department of Electrical & Electronic Engineering, The University of Hong Kong, Hong Kong, (email: swko@eee.hku.hk).

Part of this work was presented at IEEE DySPAN 2017 [2].

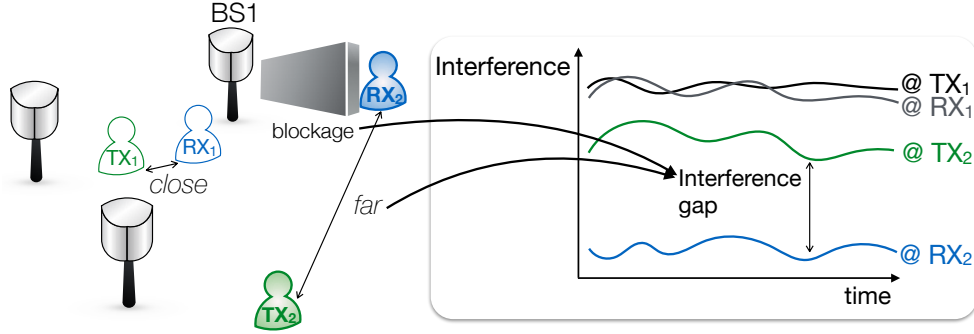


Fig. 1. Illustration of the access opportunity detection problem because of: (i) secondary TX-RX distance separation; and (ii) the blockages. When secondary TX-RX association distance is long or when there are many blockages, the SIR measured at TX significantly differs from the SIR at RX (see the SIR gap between TX_2 and RX_2), leading to detection errors.

expected to increase the spectrum utilization efficiency several-fold. Furthermore, recent advances in spectrum sensing [3] and multi-antenna techniques [4] indicate that CR may be useful to facilitate massive connectivity within the *Internet-of-Things* (IoT), a vision of next-generation communications [5].

CR features two types of users, primary and secondary, with the user status depending on their priority within a given spectrum. A secondary *transmitter* (TX) senses the medium prior to access to check spectrum utilization by primary users. However, such a sensing mechanism (triggered by the TX) has the fundamental drawback that the interference level at the secondary TX differs from that at the *receiver* (RX). This interference gap may mislead the access decision of the secondary TX, causing transmission failure. To address this issue, we develop a novel *medium access control* (MAC) termed *Sense-and-predict* (SaP), whereby each secondary TX decides to access the spectrum by predicting interference at its RX based on the sensed interference level at the TX. Specifically, the interference level at the RX is quantified as an *opportunistic probability* (OP) defined as a conditional distribution of the interference level at the secondary RX given the measured interference at the TX; the chance that the secondary TX randomly accesses the medium is the OP. Note that the OP is closely related to the spatial interference correlation between two separated locations, attributable to (i) the distance between the TX and the RX; and, (ii) blockages (see Fig. 1). We develop the spatial correlation in the form of a probability using *stochastic geometry* (SG), and use our result to obtain an accurate OP and optimize the SaP framework.

A. Prior Works

As CR seeks to address the spectrum scarcity problem, it has been extensively studied using a wide range of advanced techniques (e.g., interference alignment [6], full-duplex approaches [7], energy harvesting [8], and machine-learning [9]). The aim is to maximize the performance of secondary users while conserving the service quality of primary users. In general, it is difficult to know the positions of primary RXs, and access by secondary users is thus conservatively controlled to protect the primary users [10]. Thus, both the transmission power and range of secondary users are restricted. The interference gap between a secondary TX and its paired RX has been considered to be negligibly small. In recent CR systems, on the other hand, the prime aim is to accommodate 1,000-fold more devices in massive IoT networks. This renders the performance guarantees of secondary communications key when seeking to increase spatial reuse. Also, access by IoT devices must be carefully controlled due to their strict constraints on energy consumption and delay [5]. It is thus important to define a correct OP. To this end, the interference gap between the secondary TX and the RX must be addressed.

Specifically, two types of problems are recognized: hidden- and exposed- node problems. A hidden-node problem arises when an interferer is sensed not by the TX, but rather by the RX, and an exposed-node problem is the reverse problem [11]. These are challenging issues in the field of *carrier sensing multiple access* (CSMA) because they cause transmission failure due to a collision between two transmissions. To tackle these problems, most prior works have sought to implement additional control signals [12]–[14]. In [12], a *collision avoidance* (CA) scheme based on handshaking featured the transmission of control packets such as request-to-send, clear-to-send, and data-sending signals. In [13], a CA scheme based on a busy tone mechanism was proposed; the TX or RX sends a control packet to reserve the channel for transmission. This was extended in [14] by using an asymmetrical dual busy tone mechanism to solve the exposed-node problem. However, such additional signaling intensifies control-plane congestion when the goal is to support massive numbers of simultaneous connections. We use simple ALOHA-type random access, thus not increasing the signaling overhead, but fine-tuning the access probability depending on the level of sensed interference at the TX; we use SG to this end.

SG is accepted to be an efficient tool affording a tractable approach to interference modeling in large-scale wireless networks by focusing on analysis of a single typical point [16]. However, quantifying the spatial interference correlation using SG is far more challenging, because joint

analysis of two typical points is required [17]–[19]. The extent of correlation is highly dependent on the topological differences between the two points. For example, when the two nodes are co-located, it is obvious that they experience the same level of interference. As the distance between the nodes increases, the similarity decreases, and they finally become independent. The authors in [17] described spatial correlation in the form of a correlation coefficient in an ad hoc network. Extending such work, [18] focused on the joint coverage probability at two locations in a cellular network in which mobile devices were moving, and [19] investigated the conditional interference distribution between two locations. However, no report has yet considered blockage effects on spatial interference correlations. These are more complicated because hidden- and exposed-node problems must be considered together.

Blockages render the *line-of-sight* (LOS) conditions of each communication from interferers different at the two spatial locations, decreasing the mutual spatial interference correlation. In CR networks, this causes errors in OP detection. For example, when an interferer is in LOS to the secondary TX but not to the RX, an exposed-node problem can occur. It makes the secondary TX lose a chance to access the medium although the real interference is small. In the opposite case, a hidden-node problem occurs, causing transmission failure because interference is higher than expected. Both problems become more critical when high-frequency waves such as *millimeter-waves* (mmWs) are employed; signals are now more vulnerable to blockage [24]. The blockage effect in wireless networks has recently been investigated using SG [20]–[23]. Blockages were modeled using a Boolean approach [20], [21] or a random lattice model [22]. However, such models consider the blockage effect only in terms of single-link connectivity. Authors in [23] focused on the blockage effects on multiple links, but did not consider the effects thereof on spatial interference correlations among the links. Unlike the aforementioned works, our current study incorporates blockage effects when analyzing spatial correlations, allowing application of the SaP framework to mmW bands.

B. Contributions

In this work, we tackle the interference mismatch problem in sensing-based CR networks by exploiting the spatial correlation between the secondary TX and the RX, which is jointly affected by the locations of interferers and blockages. For example, as the secondary-pair distance increases, blockages are likely to make the LOS conditions of interferers between them more differ. In a similar vein, as the number of blockages increases, the interference gap also increases

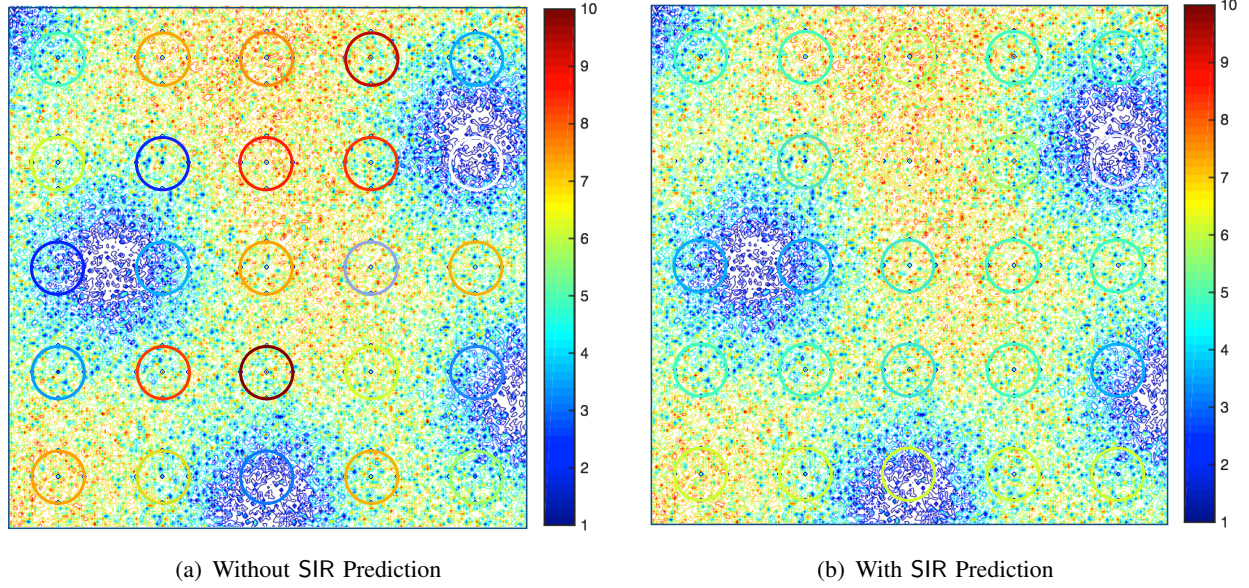


Fig. 2. The SIR prediction where the densities of the primary TXs and blockages are 10^3 TXs/km² and 10^3 buildings/km², respectively. The color represents SIR level at the corresponding location. Each secondary TX is located in the center of the circle. The circumference refers to the possible RX location separated by 2 m, of which the color is a) equal to its center in case without SIR prediction and b) predicted SIR. It is observed that the SIR prediction is so accurate that the circle is almost invisible.

even if the pair distance is identical. Our SG-based model captures such spatial correlations, thereby providing an access probability of the secondary TX. Specifically, the spatial correlation is provided in the form of a probability defined as the OP, and the secondary TX accesses the medium with that probability. It is worth noting that this probabilistic approach enables transformation of the real interference value to a value between 0 to 1, facilitating a random access design. Furthermore, the approach provides the relative levels of interference caused by various parameters, such as TX density and transmission power. For example, even if the measured interference values are equal at two different places, the OPs are not identical because of differences in network parameters, such as density and transmission power. OP enables a multiplicity of parameters to be accommodated within one metric in a probabilistic form, thus harmonizing the SaP framework.

Our principal contributions are listed below.

- **Spatial correlation analysis:** As mentioned, we capture the spatial interference correlation in the form of an OP. Regarding the distinct characteristics of wireless signal propagation, we consider two separate scenarios: below- and above-6 GHz networks (e.g., mmW network). Specifically, for a below-6 GHz network, the blockage effect disappears and we consider

only interferer locations when analyzing spatial correlations. For the above-6 GHz network, however, we consider the locations of both interferers and blockages. The results allow prediction of SIR levels at secondary RXs, as shown in Fig. 2. Furthermore, we show that the interference levels at the two locations become independent when the measured interference level is high and/or when many blockages are in place (again, in the case of the above-6 GHz network). The OP is an access probability for SaP operation; the secondary TX accesses the medium with the probability that a predicted interference level at the RX does not exceed a given access threshold. The optimality condition of utilizing OP as an access probability is also investigated.

- **SaP framework optimization:** The SaP framework is designed to maximize the *area spectral efficiency* (ASE) of the secondary network, defined as the sum of the throughput of secondary TXs within a unit area, in terms of the following two parameters: the access threshold used to decide the access probability mentioned above, and the minimum *signal-to-interference ratio* (SIR) threshold required to decode the secondary signal. Note that important design issues are in play in terms of these two parameters. For example, a small access threshold increases access probability but reduces transmission success probability because of higher aggregate interference. To compensate for such loss, we can decrease the minimum SIR but this reduces link quality. Thus, we jointly optimize the two parameters to maximize secondary network ASE while guaranteeing protection of the primary network. Some insightful observations are provided by such optimization. First, as the secondary TX density increases, the optimal access threshold increases and the lower limit of the optimal target SIR also increases. Second, the optimal access threshold decreases and target SIR increases with the building density.
- **Testbed and numerical verification:** We performed testbed experiments using universal software radio peripheral (USRP) and MATLAB simulations to verify the accuracy of our derived spatial correlations and the significant ASE improvements afforded by SaP.

The rest of this paper is organized as follows. Our system model is presented in Section II. The SaP architecture and problem formulation are presented in Section III. The OP and secondary network ASE are derived for the networks below- and above- 6 GHz in Sections IV and V, respectively. The results are evaluated using an USRP testbed and simulation under a real data-based building blockage scenario in Section VI. In addition, some realistic scenarios are briefly

discussed in Section VII. Finally, we provide concluding remarks in Section VIII followed by the proofs of lemmas and propositions (in an Appendix).

II. SYSTEM MODEL

A. Network Model

Consider a CR network where subscript $k \in \{1, 2\}$ denotes primary and secondary networks, respectively. The coordinates of the k -th network TXs follow a homogeneous Poisson point process (PPP) Φ_k with density λ_k . Processes Φ_1 and Φ_2 are mutually independent. Each secondary TX is assumed to have a paired RX at a distance of d .

We separately consider below- and above-6 GHz frequency spectra depending on the blockage effect. As mentioned, the blockage effect can be ignored in the below-6 GHz scenario but not in the above-6 GHz scenario. Blockage is modeled as follows. The distribution of blockage central point process Φ_b is stationary and isotropic in terms of density λ_b . Each blockage follows a Boolean model featuring rectangles of average length d_ℓ and width d_w . To describe the blockage effect, the LOS ball of [20] is adopted, where LOS is guaranteed if the distance is no more than the average LOS, denoted by R_L , given as:

$$R_L = \frac{\pi \sqrt{2 \exp(-\lambda_b d_\ell d_w)}}{2\lambda_b (d_\ell + d_w)}. \quad (1)$$

For simplicity, we assume that the location of the typical RX does not overlap with a blockage.

B. Channel Model

Each TX in the k -th network transmits with a power P_k . The transmitted signal experiences Rayleigh fading¹ with a mean of unity appropriate (i.e., $h \sim \exp(1)$). The primary and secondary networks share the same spectrum, causing co-channel interference. By Slyvnak's theorem [28], the SIR at a typical k -th network RX located at the origin is represented as:

$$\text{SIR}_k = \frac{P_k h^{(0)} \eta_{r^{(0)}}}{\sum_{j=1}^2 \sum_{i \in \Phi_j} P_j \phi_j^{(i)} h_j^{(i)} \eta_{r_j^{(i)}}}, \quad (2)$$

¹Although the Rayleigh model may not fit well with the real mmW environment because mmW signals are LOS-dependent, use of this model simplifies the analytical expressions and provides a lower bound for the downlink rate under conditions of Nakagami fading (see [24]–[26]). Furthermore, measurements show that small-scale fading has relatively little influence on mmW communications [27], rendering use of the Rayleigh model.

where $r^{(0)}$ and $r_j^{(i)}$ respectively represent the distances to a typical TX and TX i of the j -th network. The path-loss function η_r is given as:

$$\eta_r = \begin{cases} r^{-\alpha}, & \text{in below-6 GHz,} \\ \mathbf{1}_r r^{-\alpha}, & \text{in above-6 GHz,} \end{cases} \quad (3)$$

with the indicator function $\mathbf{1}_r$ returning unity if $r \leq R_L$ and the path-loss exponent being $\alpha > 2$. The access indicator $\phi_j^{(i)}$ is a binary variable of 1 if the i -th nearest TX of the j -th network accesses the spectrum, and 0 otherwise. Every primary TX is assumed to transmit constantly (i.e., $\phi_1^{(i)} = 1, \forall i$) whereas secondary TX transmissions depend on the MAC design (explained below).

III. SENSE-AND-PREDICT: OPERATION, OPTIMALITY AND PROBLEM FORMULATION

In this section, we introduce our proposed MAC, termed SaP where a secondary TX transmits data using OP-based random access, and we discuss on its optimality. Given the framework, the problem of maximizing the area spectral efficiency is formulated.

A. Sense-and-predict Operation

The operation of SaP is elaborated as follows. Time is slotted; each slot includes sensing and transmission periods synchronized among secondary TXs. During a sensing period, every secondary TX measures the aggregate interference, denoted by l , from the primary TXs. Assume that the sensing period is sufficiently long to enable accurate measurement of l . Each secondary TX predicts the primary interference at its paired RX separated by the distance of d conditioned on l . Specifically, assuming that the other secondary TXs are silent, $(\phi_2^{(i)})$ in (2) is zero for all i , it calculates the conditional coverage probability of the received SIR_2 larger than a threshold θ given a sensed level of interference $l = I$:

$$P = \Pr[\text{SIR}_2 > \theta | l = I, \phi_2^{(i)} = 0, \forall i], \quad (4)$$

and this is defined as the OP. The OP value P determines the random access probability of a secondary TX using an one-to-one mapping function $\mathcal{F}(x)$ to transform the level of OP to an

access probability, optimization of which will be discussed below. During a transmission period, each secondary TX accesses the medium with a probability of: $\mathcal{F}(\mathbf{P})$, namely,

$$\phi_2 = \begin{cases} 1, & \text{w.p } \mathcal{F}(\mathbf{P}), \\ 0, & \text{w.p } 1 - \mathcal{F}(\mathbf{P}). \end{cases} \quad (5)$$

B. Optimality of Opportunistic Probability Based Random Access

Given the OP value \mathbf{P} , this subsection optimizes the mapping function $\mathcal{F}(x)$ to maximize the coverage probability of a typical secondary user $\Pr[\text{SIR}_2 > \beta]$, where β is a target decoding threshold. Using an approach similar to the well-known method employed to derive network success probabilities using stochastic geometry (see e.g., SIR coverage in [15]), we obtain the following coverage probability of the secondary user, with the proof omitted for brevity:

$$\begin{aligned} \Pr[\text{SIR}_2 > \beta] &= \int_0^1 \mathcal{F}(x) x \exp(-\pi \lambda_2 d^2 \rho_0(\beta, \infty))^{\mathbb{E}[\mathcal{F}(\mathbf{P})]} f_{\mathbf{P}}(x) dx \\ &= A^{\mathbb{E}[\mathcal{F}(\mathbf{P})]} \int_0^1 \mathcal{F}(x) x f_{\mathbf{P}}(x) dx, \end{aligned} \quad (6)$$

where $\rho_0(x, t) := x^{\frac{2}{\alpha}} \int_0^t \frac{du}{1+u^{\frac{\alpha}{2}}}$, $f_{\mathbf{P}}(x)$ and $\mathbb{E}[\mathbf{P}]$ are the *probability density function* (PDF) of OP value \mathbf{P} and the expected value of OP \mathbf{P} respectively, and $A = \exp(-\pi \lambda_2 d^2 \rho_0(\beta, \infty))$. Using Hölder's inequality, we rewrite the SIR coverage as

$$\Pr[\text{SIR}_2 > \beta] \leq A^{\mathbb{E}[\mathcal{F}(\mathbf{P})]} \sqrt{\int_0^1 \mathcal{F}^2(x) f_{\mathbf{P}}(x) dx} \sqrt{\int_0^1 x^2 f_{\mathbf{P}}(x) dx}, \quad (7)$$

where the equality holds if $\mathcal{F}(x)$ and x are linearly dependent such that $\mathcal{F}(x) = cx$ at a constant c . Recalling that the coverage probability $\Pr[\text{SIR}_2 > \beta]$ is 1: plugging the above linear function into (7) and differentiating it in terms of c give the following proposition.

Proposition 1 (Optimization of a Linear Mapping Function). Among mapping functions $\mathcal{F}(x)$ whose first and second moments are identical, a linear mapping function cx achieves the maximum coverage probability of a secondary typical user when the following inequality holds:

$$\pi \lambda_2 d^2 \rho_0(\beta, \infty) > \frac{1}{\mathbb{E}[\mathbf{P}]}. \quad (8)$$

where $\rho_0(x, t)$ is specified in (6).

The above optimization condition for (8) can be satisfied when the density of the secondary

TXs λ_2 is high and the average OP $E[P]$ is small, affording a good match to the massive access required by the cognitive IoT [5], one of our target applications. We thus use the linear mapping function $\mathcal{F}(x) = x$ with $c = 1$ for notational simplicity, which has no effect on the optimal SaP design. In other words, we directly use OP P as the access probability of the secondary TX in the remainder of this paper.

C. Problem Formulation

We seek to maximize the ASE \mathcal{A} defined as the sum of the data transmission rates of the secondary RXs per unit bandwidth in a unit area [29]. To this end, the following problem is formulated:

$$\begin{aligned} \max_{\theta, \beta} \mathcal{A} &= \lambda_2 E_I[P \cdot \Pr(\text{SIR}_2 > \beta | I = I)] \ln(1 + \beta), \\ \text{s.t.} \quad \Pr[\text{SIR}_1 \leq \gamma] &\leq \tau. \end{aligned} \tag{P1}$$

where the constraint represents the primary protection requirement, such that the SIR outage probability of a primary user, $\Pr[\text{SIR}_1 \leq \gamma]$ (where γ is a target decoding threshold for a successful primary transmission) does not exceed a given constant τ . Two parameters must be optimized. One is the access threshold θ and the other is the decoding target β . Both are represented as SIR values but their corresponding usages are different. The access threshold θ controls the OP value P depending on the interference level at primary TXs. On the other hand, the decoding target β reflects the tradeoff between the coverage probability and the corresponding transmission rate considering the interference from primary and secondary TXs.

IV. SENSE-AND-PREDICT WITHOUT BLOCKAGE EFFECT

In this section, we attempt to derive a tractable form of OP by applying SG. Based on the OP, we optimize parameters of the SaP framework by solving Problem P1.

A. Opportunistic Probability Analysis

As mentioned, a secondary TX accesses the spectrum with a probability of OP P that features the spatial interference correlation between TX and RX. The direct derivation of P is intractable because the secondary TX and RX share common interferers, causing angular correlations. Such correlations violate the requirement for isotropy in point processes, blocking the use of PPP

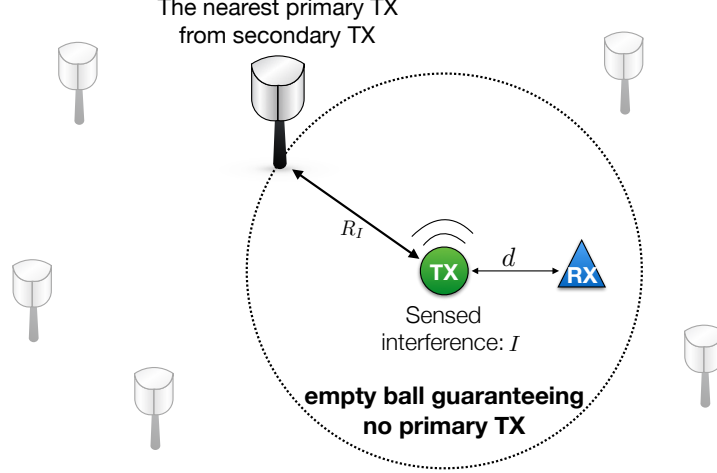


Fig. 3. A empty ball with radius R_I determined by the sensed interference level I .

techniques such as Campbell's theorem [16]. To address this issue, we introduce the following assumption:

Assumption 1 (Empty Ball). The nearest primary TX is assumed to be located on a circle with radius R defined as an *empty ball*. In other words, no primary TX exists inside the empty ball, as shown in Fig. 3. Furthermore, the other primary TXs (located outside the empty ball) are assumed to follow PPP from the perspective of a typical secondary RX.

This assumption 1 allows us to tractably manage the angular correlation problem by decomposing P into a product of two terms. The first term corresponds to the interference from the nearest primary TX on the empty ball, the angular correlation of which can be expressed using a single trigonometrical function. The second term corresponds to the aggregate interference from the other primary TXs outside the empty ball, the angular correlations of which can be disregarded because of the isotropic property of PPP. The principal result is shown in the following proposition:

Proposition 2 (OP Analysis without Blockage Effect). Assuming that the empty ball radius R is known, the OP P is given as $\mathcal{P}(R, d, \theta)$,

$$\mathcal{P}(R, d, \theta) = \frac{1}{2\pi} \int_0^{2\pi} \frac{P_2 dt}{P_2 + P_1 \theta d^\alpha (R^2 - 2dR \cos(t) + d^2)^{-\frac{\alpha}{2}}} \exp \left[- \int_{[R-d]^+}^{\infty} c_0(y) dy \right], \quad (9)$$

where $[x]^+ = \max[0, x]$, $c_0(y) = \frac{2\lambda_1 P_1 \theta d^\alpha y^{-\alpha+1}}{P_2 + P_1 \theta d^\alpha y^{-\alpha}} \arccos \left(\frac{R^2 - d^2 - y^2}{2dy} \right)$, if $|R - d| < y \leq R + d$ and

$$c_0(y) = \frac{2\pi\lambda_1 P_1 \theta d^\alpha y^{-\alpha+1}}{P_2 + P_1 \theta d^\alpha y^{-\alpha}} \text{ otherwise.}$$

Proof. See Appendix A. ■

Proposition 2 shows that the closed form of OP P can be obtained on the condition that the empty ball radius R is known. Unfortunately, determination of the exact R is impossible because many types of interferer distributions can yield the same aggregate interference. Alternatively, we approximate P by plugging the conditional expectation of R given the I , denoted by R_I , into R in (9), namely:

$$P \approx \mathcal{P}(R_I, d, \theta), \quad (10)$$

where R_I is obtained from the following problem, with the proof given in Appendix B.

$$\frac{I}{P_1} R_I^\alpha - \frac{2\pi\lambda_1}{\alpha - 2} R_I^2 - 1 = 0. \quad (11)$$

The approximation in (10) is verified by simulation to be tight (See Fig. 6 (b)). Furthermore, the closed form of R_I is enabled when the path-loss exponent $\alpha = 4$,

$$R_I = (2I)^{-\frac{1}{2}} \left(\pi\lambda_1 P_1 + [(\pi\lambda_1 P_1)^2 + 4P_1 I]^{\frac{1}{2}} \right)^{\frac{1}{2}}, \quad (12)$$

which is explicitly shown to increase with λ_1 and P_1 , and to decrease with I . We can simplify $\mathcal{P}(R_I, d, \theta)$ in (10) using the following asymptotical analysis, enabling understanding of the relationships between network parameters and the resultant OP.

Corollary 1 (Asymptotic OP). When the expected empty ball radius R_I increases, $\mathcal{P}(R_I, d, \theta)$ of (10) tends to follow $\mathcal{P}(R_I, 0, \theta)$ and finally converges to 1. On the other hand, when R_I decreases, $\mathcal{P}(R_I, d, \theta)$ decreases and converges to the following value,

$$\lim_{R_I \rightarrow 0} \mathcal{P}(R_I, d, \theta) = \mathcal{P}(0, d, \theta) = \frac{P_2 \exp \left(-\pi\lambda_1 \left(\frac{P_1 \theta d^\alpha}{P_2} \right)^{\frac{2}{\alpha}} \int_0^\infty \frac{du}{1+u^{\frac{\alpha}{2}}} \right)}{P_2 + P_1 \theta}, \quad (13)$$

which is strictly larger than zero and independent of I and R_I .

Remark 1 (Effects of Parameters). Some interesting observations arise from (12) and the Corollary 1. First, even though the same interference level is sensed, the access probability can differ depending on network parameters, including the primary TX density λ_1 and the transmission power P_1 . Second, the difference in interference level between a typical secondary

TX and an RX location falls as R_I increases, implying that a smaller I in environments with larger λ_1 and P_1 values allows secondary TXs to access the spectrum more reliably. Lastly, the fact that a non-zero lower bound of OP exists encourages the TX to access the spectrum with a certain probability, even though very large numbers of I are sensed.

B. Area Spectral Efficiency Maximization

This section deals with the ASE maximization in Problem P1, requiring an analysis of the term $E_I [P \cdot \Pr(\text{SIR}_2 > \beta | I = I)]$ as a preliminary step. Note that the OP P is given as $\mathcal{P}(R_I, d, \theta)$ in (9) at an empty ball radius of R but the conditional coverage probability $\Pr(\text{SIR}_2 > \beta | I = I)$ has not yet been derived. We express $\Pr(\text{SIR}_2 > \beta | I = I)$ in the form of $\mathcal{P}(R, d, \theta)$ in (9), and optimize θ and β tractably.

For analytical tractability, we assume that the concurrent secondary TXs are independently thinned by the average OP, denoted by $\bar{P} = E_I[P]$, and that the radius of the empty ball R is perfectly estimated, equivalent to the nearest primary TX, the PDF of which is $f_R(r) = 2\pi\lambda_1 r e^{-\pi\lambda_1 r^2}$. We can express \bar{P} in terms of $\mathcal{P}(R, d, \theta)$ of (9) as:

$$\bar{P} = \bar{\mathcal{P}}(d, \theta) = \int_0^\infty \mathcal{P}(r, d, \theta) f_R(r) dr. \quad (14)$$

Using (14), we can derive the conditional coverage probability $\Pr(\text{SIR}_2 > \beta | I)$ given in Lemma 1. In addition, this enables us to calculate the lower limit of access threshold preventing outage of a primary user; the lower limit exceeds the threshold τ , as proven in Lemma 2:

Lemma 1 (Secondary Coverage Probability). Given the access threshold θ and the radius of the empty ball R , the probability $\Pr(\text{SIR}_2 > \beta | I = I)$ is given as

$$\Pr(\text{SIR}_2 > \beta | I = I) = \mathcal{P}(R, d, \beta) \exp \left(-\pi\lambda_2 \bar{\mathcal{P}}(d, \theta) d^2 \rho_0(\beta, \infty) \right),$$

where $\rho_0(\beta, \infty)$ is specified in (6).

Proof. See Appendix C. ■

Lemma 2 (Minimum Access Threshold). To satisfy the constraint of P1, the access threshold θ should be no less than θ_{\min} that can be obtained by solving the following equation:

$$\bar{\mathcal{P}}(d, \theta_{\min}) = \frac{\lambda_1 P_2^{\frac{2}{\alpha}} [\tau + \rho(\gamma, \infty)\tau - \rho(\gamma, \infty)]}{\lambda_2 P_1^{\frac{2}{\alpha}} \rho_0(\gamma, \infty)(1 - \tau)}, \quad (15)$$

where $\rho(x, t) := x^{\frac{2}{\alpha}} \int_{x^{-\frac{2}{\alpha}}}^t \frac{du}{1+u^{\frac{\alpha}{2}}}$

Proof. See Appendix D. ■

From Lemmas 1 and 2, P1 is rewritten as

$$\max_{\theta \geq \theta_{\min}, \beta} \mathcal{A} = \ln(1 + \beta) \exp(-\pi \lambda_2 \overline{\mathcal{P}}(d, \theta) d^2 \rho_0(\beta, \infty)) \int_0^\infty \lambda_2 \mathcal{P}(r, d, \theta) \mathcal{P}(r, d, \beta) f_R(r) dr. \quad (\text{P2})$$

It is impossible to derive the closed form solution of P2 because of the complex integral term in \mathcal{A} . Using the mean value theorem, the integral term in P2 is decomposed as:

$$\int_0^\infty \lambda_2 \mathcal{P}(r, d, \theta) \mathcal{P}(r, d, \beta) f_R(r) dr = \mathcal{P}(c, d, \beta) \lambda_2 \underbrace{\int_0^\infty \mathcal{P}(r, d, \theta) f_R(r) dr}_{=\overline{\mathcal{P}}(d, \theta)}, \quad (16)$$

where c is a positive constant. Noting that $\mathcal{P}(c, d, \beta) < 1$, ASE \mathcal{A} is upper bounded as:

$$\mathcal{A} < \ln(1 + \beta) \exp(-\pi \lambda_2 \overline{\mathcal{P}}(d, \theta) d^2 \rho_0(\beta, \infty)) \lambda_2 \overline{\mathcal{P}}(d, \theta). \quad (17)$$

Instead of P1, we formulate the following problem to maximize the above upper bound as:

$$\{\theta^*, \beta^*\} = \arg \max_{\theta \geq \theta_{\min}, \beta} \ln(1 + \beta) \exp(-\pi \lambda_2 \overline{\mathcal{P}}(d, \theta) d^2 \rho_0(\beta, \infty)) \lambda_2 \overline{\mathcal{P}}(d, \theta), \quad (\text{P3})$$

which provides the relationship between the optimized parameters in a tractable form, as shown in the following proposition.

Proposition 3 (Optimal Expected OP). Given the optimal solution $\{\theta^*, \beta^*\}$ of P3, the expected OP $\overline{\mathcal{P}}(d, \theta^*)$ is given as

$$\overline{\mathcal{P}}(d, \theta^*) = \frac{1}{\pi d^2 \rho_0(\beta^*, \infty) \lambda_2}, \quad (18)$$

when $\theta^* > \theta_{\min}$.

Remark 2 (Optimal Concurrent Transmitting TX Density). This result shows that an optimal density for concurrent secondary transmissions in fact exists: $\Lambda_2^* = \lambda_2 \overline{\mathcal{P}}(d, \theta^*) = \frac{1}{\pi d^2 \rho_0(\beta^*, \infty)}$, enabling expression of the relationships between parameters. First, as λ_2 increases, the optimal access threshold θ^* should increase to retain the optimal density Λ_2^* . Second, Λ_2^* is a decreasing function of β^* . Last, as Λ_2^* should be smaller than the secondary TX density λ_2 , the optimal target β^* thus has a feasible range such that $\beta^* \geq \left[\lambda_2 \overline{\mathcal{P}}(d, \theta^*) \pi d^2 \int_0^t \frac{du}{1+u^{\frac{\alpha}{2}}} \right]^{-\frac{\alpha}{2}}$.

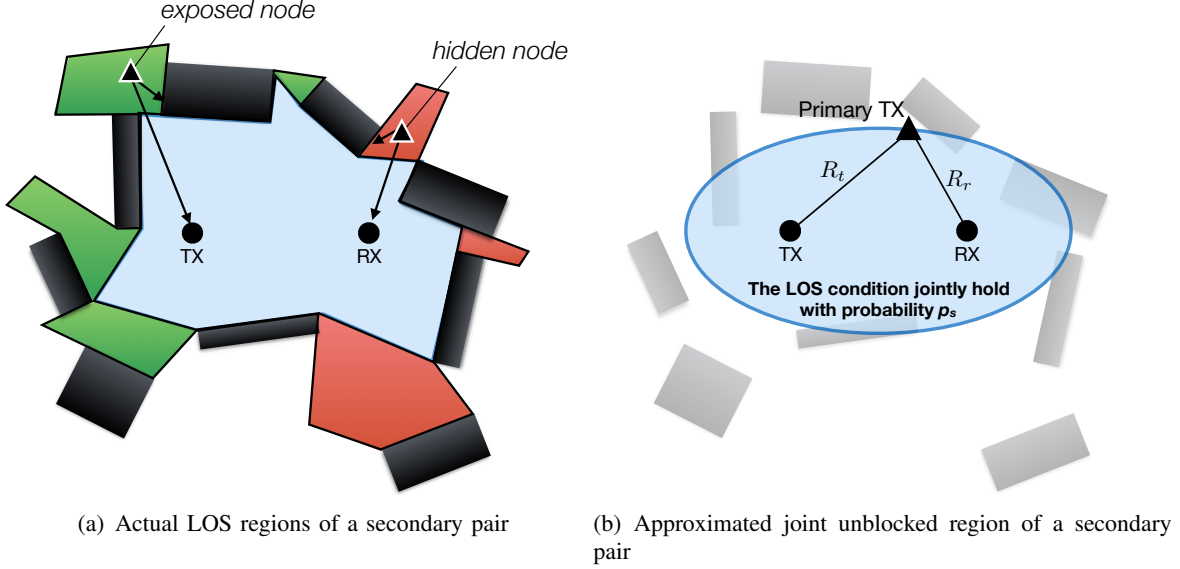


Fig. 4. Joint unblocked region of a secondary pair: assuming the LOS probabilities of two links are independent, the joint unblocked probability of a primary TX located on the ellipse with the secondary pair at two focal points is identical.

V. SENSE-AND-PREDICT WITH BLOCKAGE EFFECT

In this section, we extend the OP analysis to a case with blockage, thus the above-6 GHz scenario. Then, we maximize the corresponding ASE, providing the optimal access threshold and target SIR for decoding.

A. Opportunistic Probability Analysis

The analysis of OP incorporating the blockage effect is of prime concern in this subsection. Because of blockages, the link from a primary TX to either a secondary TX or a paired RX can be blocked, causing exposed- or hidden-node problems (See Fig. 4 (a)). To incorporate these problems into OP, we define an *unblocked probability*, denoted by p ; the probability that the link between a primary TX and a typical secondary TX or RX is unblocked. In [20], this is expressed in terms of the distance R as:

$$p(R) = \exp \left[-\frac{2\lambda_b (d_\ell + d_w)}{\pi} R \right], \quad (19)$$

where the blockage-related parameters λ_b , d_ℓ and d_w are described in Sec. II-A. For simplicity, we ignore the case in which the two links are blocked by the same blockage. A joint unblocked

probability of two links, denoted by p_u , is then represented by the product of the individual unblocked probabilities of the secondary TX and RX as:

$$p_u(R_t, R_r) = p(R_t) \cdot p(R_r) = \exp \left[-\frac{2\lambda_b (d_\ell + d_w)}{\pi} (R_t + R_r) \right], \quad (20)$$

where R_t and R_r denote the distance from a primary TX to the typical secondary TX and its RX, respectively. It is observed that p_u in (20) is not changed if the sum of the distances between the two links, $R_t + R_r$, is identical. Based on intuition, we introduce the following assumption:

Assumption 2 (Joint Unblocked Region). Both links from a primary TX to a typical secondary TX and the RX are assumed to be unblocked if the sum of their distance $R_t + R_r$ is no more than the L distance as determined by blockage-related parameters² (e.g., λ_b , d_ℓ and d_w). The geometry of the joint unblocked area is an ellipse, the two focal points of which are the secondary TX and RX locations and the major axis length the L .

Assumption 2 allows us to quantify the extent of the exposed-node problem. For example, consider one primary TX, the link of which to a typical secondary TX is unblocked. If the primary TX is within the joint unblocked region, it will also be unblocked to the paired secondary RX. Otherwise, it does not interfere with the RX, thereby causing an exposed-node problem. Note that it is straightforward to feature a hidden-node problem by considering additional interference, which is likely to not be sensed by the TX, but will be sensed by the RX. The principal result is shown in the following proposition.

Proposition 4 (OP Analysis with Blockage Effect). Assume that the empty ball radius R and the axis length L are given. Under the LOS condition between a typical secondary TX and RX, i.e., $d \leq R_L$ where R_L is specified in (1), the OP P is given by $\mathcal{P}(R, L, d, \theta)$,

$$\mathcal{P}(R, L, d, \theta) = \exp \left[-\int_{[R-d]^+}^{R_L} c_2(y) dy \right] \cdot \begin{cases} \int_0^\pi \frac{P_2 \pi^{-1} dt}{P_2 + P_1 \theta d^\alpha (R^2 - 2dR \cos(t) + d^2)^{-\frac{\alpha}{2}}} & \text{if } R < \frac{L}{2} - \frac{d}{2}, \\ \int_0^u \frac{P_2 \pi^{-1} dt}{P_2 + P_1 \theta d^\alpha (R^2 - 2dR \cos(t) + d^2)^{-\frac{\alpha}{2}}} + \frac{\pi - c}{\pi} & \text{if } \frac{L}{2} - \frac{d}{2} \leq R < \frac{L}{2} + \frac{d}{2}, \\ 1 & \text{if } \frac{L}{2} + \frac{d}{2} \leq R, \end{cases} \quad (21)$$

² The distance L can be obtained via data curve-fitting based on real geometric data, as will be described in Section VI-C.

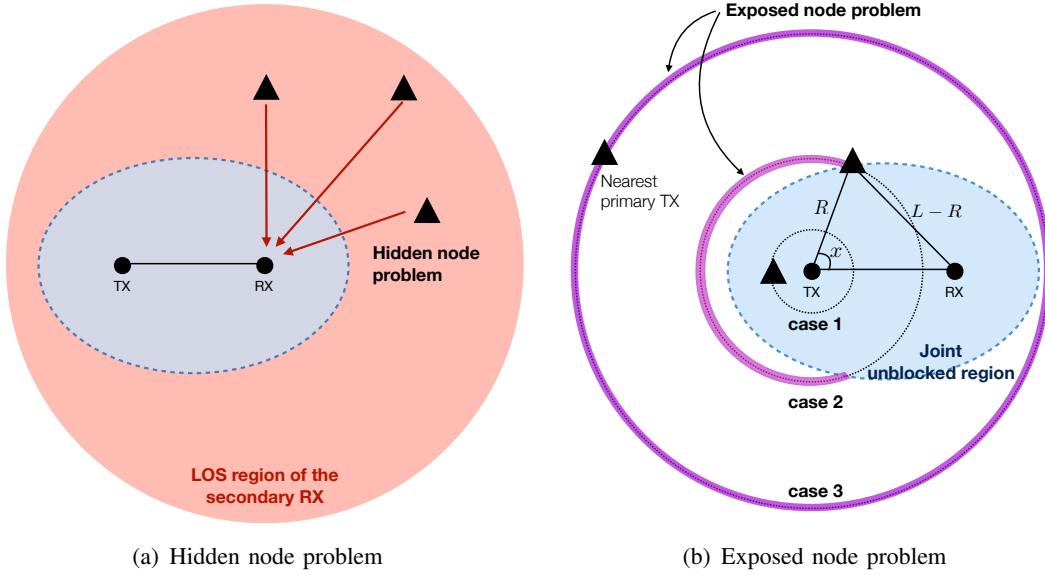


Fig. 5. Joint unblocked region and exposed/hidden node problem.

where $c_2(y) = \frac{2\lambda_1 P_1 \theta d^\alpha y^{-\alpha+1}}{P_2 + P_1 \theta d^\alpha y^{-\alpha}} \arccos\left(\frac{R^2 - d^2 - y^2}{2dy}\right)$ if $\min(R_L, |R - d|) < y \leq \min(R_L, R + d)$ and $c_2(y) = \frac{2\pi\lambda_1 P_1 \theta d^\alpha y^{-\alpha+1}}{P_2 + P_1 \theta d^\alpha y^{-\alpha}}$ otherwise, and $u = \arccos\left(\frac{d^2 + 2LR - L^2}{2dR}\right)$. It is obvious that $\mathcal{P}(R, L, d, \theta)$ is zero if $d > R_L$.

Proof. See Appendix E. ■

Remark 3 (Hidden and Exposed Node Problems). The first part of (21) represents the SIR coverage considering the aggregate interference from all primary TXs except the nearest TX, including TXs with hidden-node problems (see Fig. 5(a)). The second part of the term represents the SIR coverage considering interference from the nearest primary TX imposed on the secondary TX, by capturing whether or not this is an exposed node with respect to the secondary RX (see Fig. 5(b)). Specifically, we consider the following three cases depending on the distance between the secondary TX and the nearest primary TX R , namely: **Case 1**) no exposed-node problem occurs when $R < \frac{L}{2} - \frac{d}{2}$; **Case 2**) a partial problem occurs when $\frac{L}{2} - \frac{d}{2} \leq R < \frac{L}{2} + \frac{d}{2}$; and, **Case 3**) a problem always occurs when $\frac{L}{2} + \frac{d}{2} \leq R$ ³. The possibility that the nearest primary TX causes an exposed-node problem decreases as the distance R increases, equivalent to low-level

³In Case 3, the nearest primary TX could be regarded as an exposed node even though it is closer to the secondary RX than is the secondary TX, creating an error in the OP analysis. Fortunately, such an error is marginal because the interference level of Case 3 is quite small, and the resultant OP $\mathcal{P}(R, L, d, \theta)$ is nearly unity despite the error.

interference I .

Remark 4 (Effect of Blockages on OP). As blockages become larger and/or denser, the axis length L decreases and the second part of the OP (21) becomes close to unity. This implies that when blockage size or density is high, the correlation between interference at the secondary TX and RX decreases (i.e., the measured interference I has less impact on the OP). However, as the blockage size or density decreases, the axis length $L \rightarrow \infty$, and the LOS distance $R_L \rightarrow \infty$; and the OP with blockage effect (21) becomes identical to that without (9) in Section IV.

As in the case without blockage, we approximate P by replacing the exact R with its expected value, namely:

$$P \approx \mathcal{P}(R_I, L, d, \theta), \quad (22)$$

where R_I is straightforwardly derived when modifying the upper limit of integration in (37) from ∞ to R_L , as follows.

$$\left(\frac{I}{P_1} + \frac{2\pi\lambda_1}{\alpha - 2} R_L^{2-\alpha} \right) R_I^\alpha - \frac{2\pi\lambda_1}{\alpha - 2} R_I^2 - 1 = 0. \quad (23)$$

Furthermore, the distance R_I is derived as a closed-formula as in the following cases according to the path-loss exponent α ,

$$\lim_{\alpha \rightarrow 2+} R_I = \left[\frac{I}{P_1} - 2\pi\lambda_1 \log(R_L) \right]^{-\frac{1}{2}}, \quad (24)$$

$$\lim_{\alpha \rightarrow 4} R_I = \left(\pi\lambda_1 P_1 + [(\pi\lambda_1 P_1)^2 + 4P_1 (I + \pi\lambda_1 P_1 R_L^{-2})] \right)^{\frac{1}{4}} [2 (I + \pi\lambda_1 P_1 R_L^{-2})]^{-\frac{1}{2}}. \quad (25)$$

Note that Remark 1 is still valid in case with blockage effect.

B. Area Spectral Efficiency Maximization

In this section, we seek to provide ASE-maximizing access thresholds θ and SIR target β when blockage effect is considered. The ASE with blockage effect is given, via some modifications of the ASE without blockage, in Section IV-B by considering the void probability that the nearest interferer is outside the range of R_L as in [21]. Then, the ASE is represented as follows:

$$\mathcal{A} = \frac{\exp(-\pi\lambda_2 \overline{\mathcal{P}}(L, d, \theta) d^2 \rho_0(\beta, R_L)) \ln(1 + \beta)}{1 - \exp(-\pi\lambda_1 R_L^2)} \int_0^{R_L} \mathcal{P}(r, L, d, \theta) \mathcal{P}(r, L, d, \beta) f_R(r) dr. \quad (26)$$

where $\overline{\mathcal{P}}(L, d, \theta) = \int_0^{R_L} \frac{\mathcal{P}(r, L, d, \theta) f_R(r)}{1 - \exp(-\pi \lambda_1 R_L^2)} dr$ denotes the average OP with blockage effect.

As in P3, we reformulate the optimization problem to maximize the upper bound of the ASE in the presence of blockage. With the aid of the mean value theorem, the probability $\mathcal{P}(r, L, d, \beta)$ in (26) is detached from the integration, representing the upper bound of ASE as follows:

$$\mathcal{A} < \frac{\exp(-\pi \lambda_2 \overline{\mathcal{P}}(L, d, \theta) d^2 \rho_0(\beta, R_L)) \ln(1 + \beta)}{1 - \exp(-\pi \lambda_1 R_L^2)} \lambda_2 \overline{\mathcal{P}}(L, d, \theta). \quad (27)$$

This enables the problem formulation as

$$\{\theta^*, \beta^*\} = \arg \max_{\theta \geq \hat{\theta}_{\min}, \beta} \frac{\exp(-\pi \lambda_2 \overline{\mathcal{P}}(L, d, \theta) d^2 \rho_0(\beta, R_L)) \ln(1 + \beta)}{1 - \exp(-\pi \lambda_1 R_L^2)} \lambda_2 \overline{\mathcal{P}}(L, d, \theta), \quad (P4)$$

where the minimum access threshold $\hat{\theta}_{\min}$ is derived by solving the following equation:

$$\overline{\mathcal{P}}(L, d, \hat{\theta}_{\min}) = \frac{\lambda_1 P_2^{\frac{2}{\alpha}} [\tau + \rho(\gamma, R_L) \tau - \rho(\gamma, R_L)]}{\lambda_2 P_1^{\frac{2}{\alpha}} \rho_0(\gamma, R_L) (1 - \tau)}, \quad (28)$$

representing that $\hat{\theta}_{\min}$ decreases with the blockage density and size.

Proposition 5 (Optimal Expected OP with Blockage Effect). The optimal expected OP $\overline{\mathcal{P}}(L, d, \theta^*)$ is given as

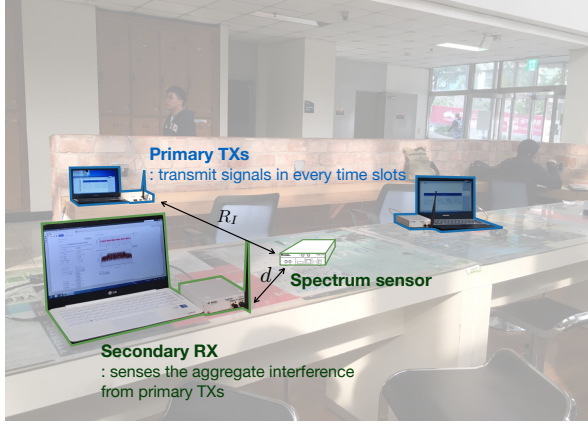
$$\overline{\mathcal{P}}(L, d, \theta^*) = \frac{1}{\pi d^2 \rho_0(\beta, R_L) \lambda_2}, \quad (29)$$

when $\theta^* > \hat{\theta}_{\min}$.

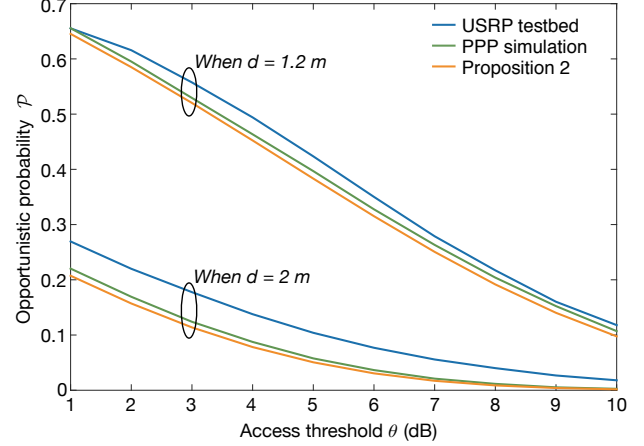
Remark 5 (Effect of Blockages). The optimal density of concurrent secondary transmissions, $\Lambda_2^* = \lambda_2 \overline{\mathcal{P}}(L, d, \theta^*) = \frac{1}{\pi d^2 \rho_0(\beta, R_L)}$, depends on blockage density and size. Large or densely deployed blockages reduce the LOS distance R_L , in turn reducing $\rho_0(\beta, R_L)$ in (29). Also, the optimal density Λ_2^* increases; thus, the optimal access threshold θ^* should be decreased to retain optimal transmission density. On the other hand, the target β^* should be increased to reflect the reduced interference and the correspondingly increased transmission success probability.

VI. PERFORMANCE EVALUATIONS

In this section, the analytical SaP design results are evaluated using a USRP testbed and simulations.



(a) The USRP testbed setup for CR networks



(b) Result comparison

Fig. 6. OP with SaP according to threshold θ ($R_I = 3.6$ m, $\lambda_1 = 7 \times 10^3$ TXs/km², $P_1 = 11.3$ dBm, $P_2 = 5$ dBm, $\alpha = 3$).

A. Opportunistic Probability Verification by USRP Testbed Experiments

To verify the derived OP in Proposition 2, we compare the values with measurements derived using a real testbed featuring three laptops and three USRPs (NI-USRP 2900), as shown in Fig. 6(a). Each laptop was connected to a USRP via a USB 3.0 connection, and controlled the USRP employing LabVIEW Communications 2.0 software. The primary network comprised two USRPs (two primary TXs), each of which transmitted a signal of 11.3 dBm at a center frequency of 1.3 GHz in every time slot, with a bandwidth of 200 kHz. The secondary network featured one USRP (a secondary RX). Because of the limited number of USRP devices, we assumed the existence of a virtual secondary TX transmitting a signal of power 5 dBm at same carrier frequency as that of the primary TXs. The laptops were used to configure the paired USRP devices. The distance R_I between the secondary TX and the nearest primary TX was 3.6 m. The secondary RX measured the aggregate interference from the primary TXs with a sensing bandwidth of 600 kHz, and passed the signal to a lowpass filter with a bandwidth of 400 kHz. The RX gain was 61 dB. At the measured interference level, the secondary RX calculated its SIR assuming that the signal from the virtual secondary TX experienced only path-loss attenuation.

We also performed MATLAB simulations. We considered a square of 1×1 km² where the primary TX density was λ_1 , the transmission powers P_1 and P_2 , and the distance R_I identical to that of the USRP testbed experiments. The path-loss exponent was set to 3 considering that the testbed experiments were performed indoors. Fig. 6(b) shows that the analytical OP from

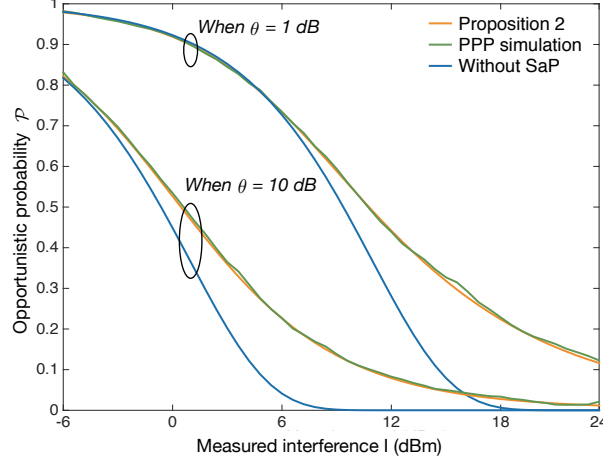


Fig. 7. OP according to the measured interference I ($\lambda_1 = 5 \times 10^2$ TXs/km², $d = 2$ m).

Proposition 2 is relatively consistent with that of the PPP simulation. A slight difference is apparent, but the tendencies are similar. The reason why access probabilities from the USRP testbed are higher than those of analysis is because two primary TXs do not adequately represent a real primary network comprising a near-infinite number of TXs. This renders secondary RX measures of aggregate interference lower than those of analysis and PPP simulation, yielding an increment in SIR coverage. This gap would be mitigated by increasing USRP numbers and/or the experimental area.

B. Opportunistic Probability and Area Spectral Efficiency Maximization without Blockage Effect

This section verifies the OP and ASE calculations in the absence of blockage (i.e., in the below-6 GHz scenario). The simulation parameters had the following default settings unless specified otherwise: Transmission powers of the primary and secondary TXs $P_1 = 43$ dBm and $P_2 = 23$ dBm, respectively, and a path-loss exponent α of $\alpha = 4$.

Fig. 7 presents the OP in terms of the measured interference I . As I increases, the OP decreases, showing that the analytical results were in good agreement with the simulated results. Here, the OP in the absence of SaP represents the predicted SIR coverage when the interference level at RX was identical with that at TX, I . The OP gap with and without SaP increases with I because of the weakened interference correlation between the secondary TX and the RX (see Corollary 1). This implies that SaP can reduce the number of false alarms (when the secondary TX decides not to access the spectrum because of measured high interference, even

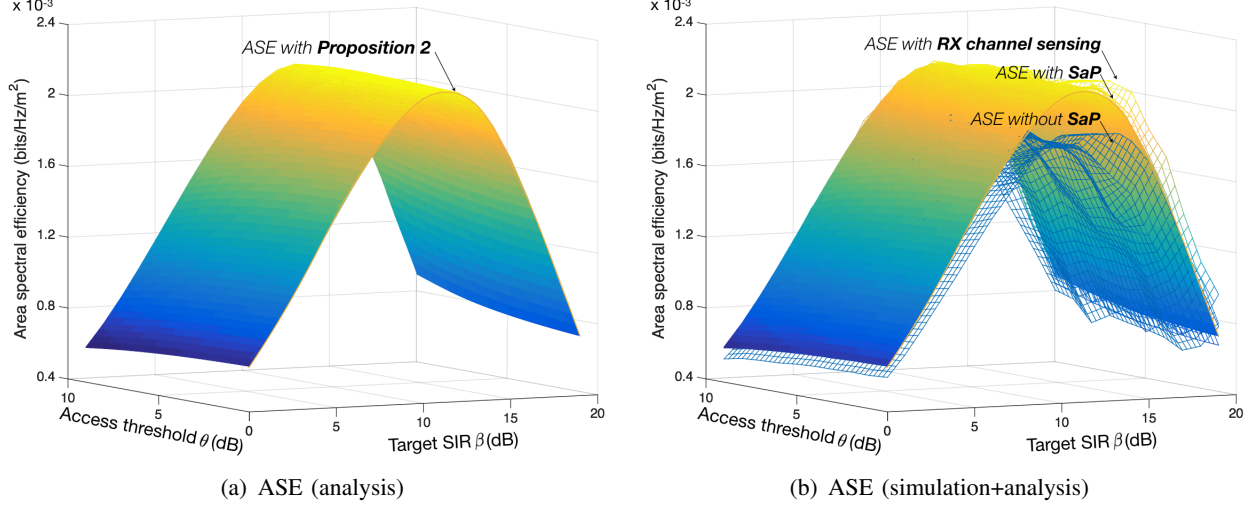


Fig. 8. ASE analysis and simulation ($\lambda_1 = 5 \times 10^2$ TXs/km², $\lambda_2 = 200$ TXs/km², $d = 2$ m).

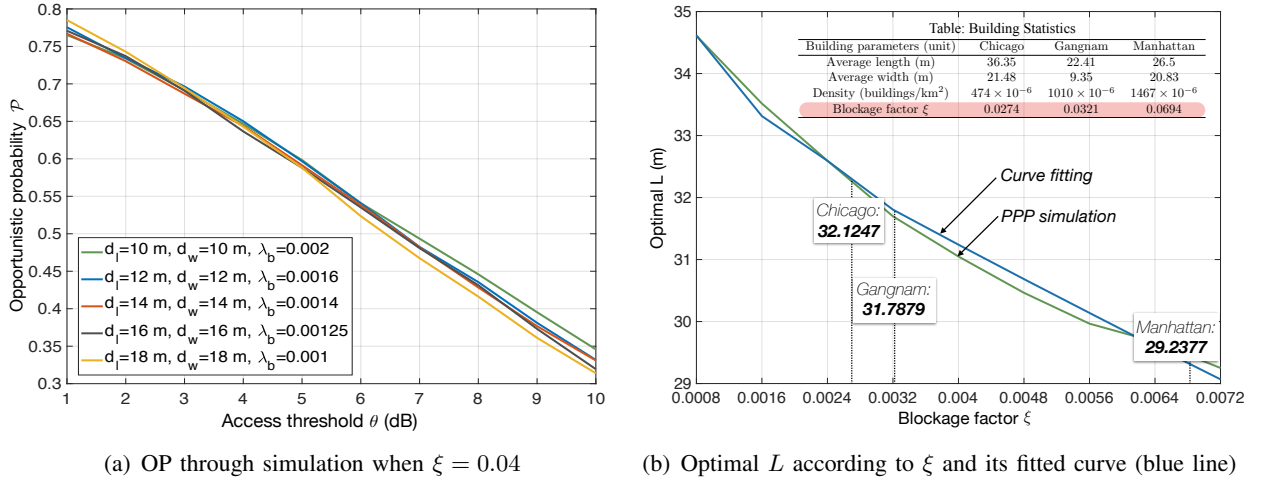


Fig. 9. OP with blockage effect and optimal distance of joint unblocked ellipse area, L ($\lambda_1 = 3 \times 10^2$ TXs/km², $\lambda_2 = 1 \times 10^2$ TXs/km², $d = 5$ m)

if the interference is in fact low).

Fig. 8 shows that the analytical and simulated ASE are well-matched, validating the analysis. Compared to the simulated ASE without SaP, the proposed SaP affords a much higher ASE, close to the ASE associated with RX channel sensing, which is regarded as optimal.

C. Opportunistic Probability and Area Spectral Efficiency Maximization with Blockage Effect

Before comparing analytical and simulation results, it is necessary to determine the axis length L in (21) using 2D blockage geometrical information. Recalling that LOS condition depends

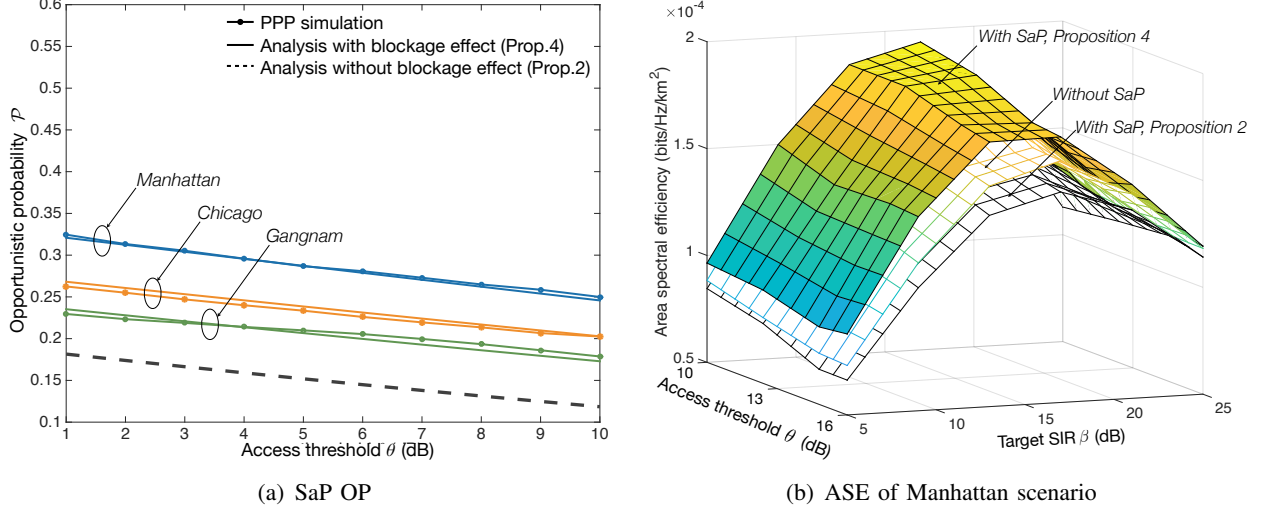


Fig. 10. OP and ASE of SaP ($\lambda_1 = 3 \times 10^2$ TXs/km², $\lambda_2 = 1 \times 10^2$ TXs/km², $d = 5$ m)

on $\lambda_b(d_l + d_w)$ (see (20)), we first define a blockage factor $\xi = \lambda_b(d_l + d_w)$. We then check whether it is appropriate to use the blockage factor ξ in simulations with different values of λ_b , d_l , and d_w that yield the same ξ (see Fig. 9(a)). We then find the axis length L that affords the smallest gap between the OP results from PPP simulation and analysis of (21), and create a fitted curve of optimal L against ξ as follows: $L = 10^9 \exp(-2583\xi) + 34.16 \exp(-2.242\xi)$, where the *sum of squared errors* (SSE) is 0.362. Armed with this result, we calculate the optimal L s of three cities: Chicago, Gangnam, and Manhattan, as shown in Fig. 9(b). Relevant parameters (density, and average length and width) are summarized in the Table of Fig. 9(b).

Fig. 10(a) illustrates access probabilities according to the three city scenarios. There is a gap between OP from Proposition 4 and the simulation result, but the gap is so small to be negligible. It also shows that the OP of Proposition 2 is quite different to those of Proposition 4 and simulation, emphasizing to consider the blockage effect.

Fig. 10(b) verifies the ASE improvement with the SaP algorithm, as revealed by MATLAB simulation. In addition, using the OP from Proposition 2 yields the lowest ASE, implying that OP predicted without considering the blockages even decreases the secondary performance than when using the TX sensing result directly. This indicates that considering the blockage effect is highly important to provide an appropriate OP, especially in an urban area like Manhattan.

VII. DISCUSSIONS

In this section, we discuss on some considerations to operate SaP in practical environments.

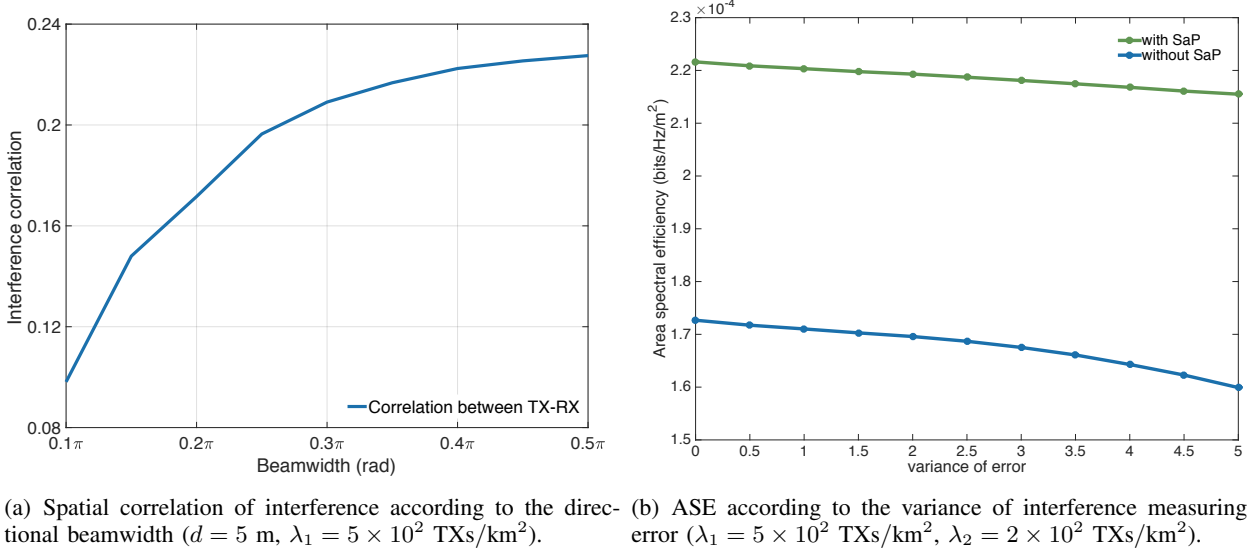


Fig. 11. Impact of beamwidth and interference measurement error.

A. Impact of Directional Transmission in CR Networks

When each TX utilizes a directional antenna, as in an mmW network, the spatial correlation of interference between the secondary TX and the RX decreases as the signal from a primary TX may interfere with only one node. In this case, both hidden- and exposed-node problems more frequently occur, intensifying OP errors (see Fig. 11(a)). This implies that more complex OP analysis is required, perhaps including beamwidth effects, as the probability that a TX interferes with a secondary TX and the RX simultaneously increases with the beamwidth. If the beam signal is very sharp, the interference correlation becomes extremely low, indicating that a random access scheme may be appropriate for CR networks rather than the conventional channel-sensing-based MAC scheme.

B. Interference Measurement

In practice, interference measurement errors can be caused by practical limitations in sensing circuit design. This may create errors in calculation of spectrum access OPs, decreasing CR network performance. To quantify such problems, we measured ASEs by simulation when measurement errors were modeled as normal distributions with zero means; the variance represents the error level. Fig. 11(b) shows that SaP still affords significant ASE improvements. ASE in the absence of SaP decreased more rapidly than does ASE in the presence of SaP, implying that SaP is more robust to interference measurement errors than is the conventional TX sensing

method. The reason behind is that the SaP considers primary network parameters such as TX density and power, enabling calibration of incorrect interference to some extent.

C. Path-Loss Exponent

Recall that all derivations of this paper are based on the assumption that a path-loss model is appropriate. We used a simplified single-slope path-loss model where large-scale signal attenuation depends on a single path-loss exponent that changes depending on the environment (e.g., antenna selection, cell type, or frequency band). It is essential to trace the exponent consistently via algorithms estimating the mean interference [31] or the internode distance [32]. In addition, it is worth considering future extensions to the more realistic path-loss models such as multi-slope models [33] or ray tracing [34].

D. Primary TX Density

The primary TX density is another important factor that must be estimated not only to calculate the aggregate interference of a secondary RX, but also to guarantee the service quality of the primary user. There are two ways by which to acquire primary TX density: i) periodical update by the network (e.g., DTV or LTE systems) [35]; and ii) estimations based on statistical techniques, such as a maximum-likelihood method assessing received powers [36].

VIII. CONCLUSION

We tackled the problem of detecting spectrum access in CR networks posed by the interference gap between secondary TXs and the RX, caused by differences in location and blockage. We developed an SaP protocol whereby the interference level at the secondary RX is predicted based on channel measurement by its paired TX. SG has been applied to quantify the spatial interference difference in the form of the SIR coverage probability, defined as the OP, which is directly used for ALOHA-based random access with optimization. Based on the SaP framework, the access threshold and target SIR are jointly optimized to maximize secondary network ASE while protecting the service quality of the primary network, providing useful insights in terms of SaP design.

This work can be extended in several interesting ways to further improve the SaP framework. First, we could consider cooperative sensing among secondary TXs, which is known to outperform non-cooperative sensing, but at a cost of increased energy consumption [37]. Second, the

use of machine-learning techniques to track environmental changes would align with the recent research interests of those studying wireless communications. Last, the use of more advanced physical layering techniques (e.g., compressive sensing and full duplexing) is promising.

APPENDIX

A. Proof of Proposition 2

Let the value x denote the distance between a typical secondary RX and T_1 . Then the OP is represented as:

$$\Pr \left[\frac{P_2 h^{(0)} d^{-\alpha}}{P_1 \left(h x^{-\alpha} + \sum_{i \in \Phi_1 \setminus T_1} h^{(i)} x_1^{(i)-\alpha} \right)} > \theta \right] \quad (30)$$

$$= \mathbb{E}_{x,h} \left[\exp \left(-\frac{\theta P_1 d^\alpha h x^{-\alpha}}{P_2} \right) \right] \times \mathbb{E}_{\Phi_1, \{h^{(i)}\}} \left[\exp \left(-\frac{\theta P_1 d^\alpha \sum_{i \in \Phi_1 \setminus T_1} h^{(i)} x_1^{(i)-\alpha}}{P_2} \right) \right]. \quad (31)$$

Utilizing that the fading $h \sim \exp(1)$ provides

$$\mathbb{E}_{x,h} \left[\exp \left(-\frac{\theta P_1 h d^\alpha x^{-\alpha}}{P_2} \right) \right] = \mathbb{E}_x \left[\frac{P_2}{P_2 + \theta P_1 d^\alpha x^{-\alpha}} \right] \quad (32)$$

$$= \frac{1}{2\pi} \int_0^\infty \frac{P_2}{P_2 + P_1 \theta d^\alpha (R_I^2 - 2dR_I \cos(i) + d^2)^{-\frac{\alpha}{2}}} di, \quad (33)$$

where the last step follows from the triangular function appropriate when the angle between the primary TX T_1 and a typical secondary RX has a uniform distribution. Under the empty ball condition, we know that there is an empty ball of radius R_I with no primary TX inside. Imagine a thin circular ring B_y of radius y around a secondary RX. The secondary RX does not have any interferer within the area intersecting B_y and the empty ball. Then, the intensity function of the interferer becomes:

$$\lambda' = \begin{cases} 0 & \text{if } 0 < y \leq \max(0, r - d), \\ 2 \arccos \left(\frac{R_I^2 - d^2 - y^2}{2dy} \right) \lambda_1 y & \text{if } \max(0, R_I - d) < y \leq R_I + d, \\ 2\pi \lambda_1 y & \text{if } R_I + d < y. \end{cases} \quad (34)$$

Applying (34) and probability generating function of PPP, the right part of (31) becomes

$$\begin{aligned} & \mathbb{E}_{\Phi_1, \{h^{(i)}\}} \left[\exp\left(-\frac{\theta P_1 d^\alpha \sum_{i \in \Phi_1 \setminus T_1} h^{(i)} x_1^{(i)-\alpha}}{P_2}\right) \right] \\ &= \exp \left(-\lambda_1 \int_0^\infty \frac{2\pi P_1 \theta d^\alpha y^{-\alpha+1}}{P_2 + P_1 \theta d^\alpha y^{-\alpha}} dy + \lambda_1 \int_{|R_I-d|}^{R_I+d} \frac{2 \left(\frac{R_I^2 - d^2 - y^2}{2dy} \right) P_1 \theta d^\alpha y^{-\alpha+1}}{P_2 + P_1 \theta d^\alpha y^{-\alpha}} dy \right) \\ & \quad \times \exp \left(-\lambda_1 \int_{\min(0, R_I-d)}^{R_I-d} \frac{2\pi P_1 \theta d^\alpha y^{-\alpha+1}}{P_2 + P_1 \theta d^\alpha y^{-\alpha}} dy \right). \end{aligned} \quad (35)$$

Plugging (33) and (35) into (31) finalizes the proof.

B. Proof of R_I without Blockage Effect

When the distance between a typical secondary TX and its nearest primary TX is equal to R_I , the expected interference is represented using Campbell's theorem [16] as:

$$P_1 \mathbb{E}_h [h R_I^{-\alpha}] + \underbrace{P_1 \mathbb{E}_{\Phi_1, \{h^{(i)}\}} \left[\sum_{i \in \Phi_1 \setminus T_1} h^{(i)} x_1^{(i)-\alpha} \right]}_{(a)}, \quad (36)$$

where T_1 denotes the nearest primary TX. Let I_r denote $\sum_{i \in \Phi_1 \setminus T_1} h^{(i)} x_1^{(i)-\alpha}$ in (a). In order to derive (a), we consider the Laplace transform of I_r , $\mathcal{L}(s) = \mathbb{E} [e^{-s I_r}]$.

$$\mathcal{L}(s) = \mathbb{E}_{\Phi_1} \left[\prod_{i \in \Phi_1 \setminus T_1} \mathbb{E}_{h^{(i)}} \left(e^{-s h^{(i)} x_1^{(i)-\alpha}} \right) \right] \stackrel{(b)}{=} \exp \left(-2\pi \lambda_1 \mathbb{E}_h \left[\int_{R_I}^\infty (1 - \exp(-s h r^{-\alpha})) r dr \right] \right) \quad (37)$$

$$\stackrel{(c)}{=} \exp \left(-\pi \lambda_1 \mathbb{E}_h \left[\int_0^{R_I^{-\alpha}} \frac{t^{-\frac{2}{\alpha}} s h dt}{e^{s h t}} - r^2 (1 - e^{-s h r^{-\alpha}}) \right] \right) \quad (38)$$

where (b) follows from the probability generating function of PPP [16] and (c) from the partial integral. By applying that $\mathbb{E} [I_r] = -\frac{\partial}{\partial s} \mathcal{L}(s)|_{s=0}$, the function (a) is represented as $\frac{2P_1 \pi \lambda_1 \mathbb{E}[h] R_I^{2-\alpha}}{\alpha-2}$. Now that $h \sim \exp(1)$, finding R_I that satisfies $I = P_1 R_I^{-\alpha} + \frac{2P_1 \pi \lambda_1 R_I^{2-\alpha}}{\alpha-2}$ finalizes the proof.

C. Proof of Lemma 1

Now that the signal experiences the Rayleigh fading, the success probability is divided into:

$$\Pr(\text{SIR}_2 > \beta|I) = \Pr\left(\frac{h^{(0)}d^{-\alpha}P_2}{\sum I_1} > \beta|I\right) \Pr\left(\frac{h^{(0)}d^{-\alpha}P_2}{\sum I_2} > \beta|I\right), \quad (39)$$

where $\sum I_1$ denotes the sum of interference from primary TXs and $\sum I_2$ the sum of interference from secondary TXs, respectively. The first probability is directly calculated from the OP. For deriving the second probability, we assume that transmitting secondary TXs are independently thinned with $\overline{\mathcal{P}}(\theta)$. Applying mapping theorem [16] in SIR coverage [15] completes the proof.

D. Proof of Lemma 2

From the outage probability derived by using the Theorem 2 in [15], we represent the outage probability of the primary network as:

$$\Pr[\text{SIR}_1 \leq \gamma] = 1 - \frac{\lambda_1 P_2^{\frac{2}{\alpha}}}{\lambda_2 \overline{\mathcal{P}}(\theta) \rho_0(\gamma, \infty) P_1^{\frac{2}{\alpha}} + \lambda_1 P_2^{\frac{2}{\alpha}} (\rho(\gamma, \infty) + 1)}, \quad (40)$$

where $\rho_0(x, t) := x^{\frac{2}{\alpha}} \int_0^t \frac{du}{1+u^{\frac{\alpha}{2}}}$ and $\rho(x, t) := x^{\frac{2}{\alpha}} \int_{x^{-\frac{2}{\alpha}}}^t \frac{du}{1+u^{\frac{\alpha}{2}}}$. Reminding the protection condition that $\Pr[\text{SIR}_1 \leq \gamma] < \tau$ finalizes the proof.

E. Proof of Proposition 4

By reference to the empty ball radius R , we consider three cases. First, when $R < \frac{L}{2} - \frac{d}{2}$, the T_1 is in the joint unblocked region. Thus the signal from T_1 interferes with the secondary RX, the interference power of which is derived using a triangular function as in (33). Next, when $\frac{L}{2} - \frac{d}{2} \leq R < \frac{L}{2} + \frac{d}{2}$, T_1 interferes with the secondary RX if that RX is within the ellipse area (the purple region in Fig. 5). Otherwise, T_1 does not interfere with the secondary RX, causing an exposed-node problem (red region in Fig. 5). The angle, x , between the major axis and the line between the secondary TX and T_1 when T_1 is located at the intersection of the empty ball and the joint unblocked region, is derived from $d^2 - 2dR \cos(x) + R^2 = (L - R)^2$ as follows:

$$x = \arccos\left(\frac{d^2 + 2LR - L^2}{2dR}\right) \quad (41)$$

Thus, when the angle t in (33) is smaller than x of (41), the primary TX interferes with the secondary RX with an interference power derived as in (33). Last, when $\frac{L}{2} - \frac{d}{2} \leq R < \frac{L}{2} + \frac{d}{2}$, T_1 cannot interfere with the secondary RX. Thus, the interference power becomes 0. In terms of

aggregate interference from primary TXs outside the empty ball, the fact that interferers located further than R_L from the secondary RX cannot interfere yields the final result.

REFERENCES

- [1] S. Haykin, "Cognitive radio: Brain-empowered wireless communications," *IEEE J. Sel. Areas Commun.*, vol. 23, no. 2, pp. 201–220, Feb. 2005.
- [2] J. Kim, S.-W. Ko, H. Cha, and S.-L. Kim, "Sense-and-predict: opportunistic MAC based on spatial interference correlation for cognitive radio networks," in *Proc. IEEE DySPAN*, Baltimore, MD, USA Mar. 2017.
- [3] T. Ycek and H. Arslan, "A survey of spectrum sensing algorithms for cognitive radio applications," *IEEE Commun. Surveys Tuts.*, vol. 11, no. 1, pp. 116–130, First Quart., 2009.
- [4] G. Scutari, D. P. Palomar, and S. Barbarossa, "Cognitive MIMO radio," *IEEE Signal Process. Mag.*, vol. 25, no. 6, pp. 46–59, Nov. 2008.
- [5] E. Dahlman, G. Mildh, S. Parkvall, J. Peisa, J. Sachs, Y. Seln, and J. Skld, "5G wireless access: Requirement and realization," *IEEE Commun. Mag.*, vol. 52, no. 12, pp. 42–47, Dec. 2014.
- [6] S.-J. Kim and G. B. Giannakis, "Optimal resource allocation for MIMO ad hoc cognitive radio networks," *IEEE Trans. Inf. Theory*, vol. 57, no. 5, pp. 3117–3131, May 2011.
- [7] M. Amjad, F. Akhtar, M. H. Rehmani, M. Reisslein, and T. Umer, "Full-duplex communication in cognitive radio networks: A survey," *IEEE Commun. Surveys Tuts.*, vol. 19, no. 4, pp. 2158–2191, Fourth Quart., 2017.
- [8] S. Lee, R. Zhang, and K. Huang, "Opportunistic wireless energy harvesting in cognitive radio networks," *IEEE Trans. Wireless Commun.*, vol. 12, no. 9, pp. 4788–4799, Sep. 2013.
- [9] M. Bkassiny, Y. Li, and S. K. Jayaweera, "A survey on machine-learning techniques in cognitive radios," *IEEE Commun. Surveys Tuts.*, vol. 15, no. 3, pp. 1136–1159, Third Quart., 2013.
- [10] Q. Zhao, and B. M. Sadler, "A survey of dynamic spectrum access," *IEEE Signal Process. Mag.*, vol. 24, no. 3, pp. 79–89, May 2007.
- [11] L. Boroumand, R. H. Khokhar, L. A. Bakhtiar, and M. Pourvahab, "A review of techniques to resolve the hidden node problem in wireless networks," *Smart Computing Review*, vol. 2, no. 2, pp. 95–110, Apr. 2012.
- [12] K. Liu, S. Leng, H. Fu, and L. Li, "A novel dual busy tone aided mac protocol for multi-hop wireless networks," in *Proc. IEEE International Conference on Dependable, Autonomic and Secure Computing*, Chengdu, China, Dec. 2009.
- [13] C. Wu and V. O. K. Li, "Receiver-initiated busy-tone multiple access in packet radio networks," in *Proc. ACM SIGCOMM*, 1987.
- [14] B. Shrestha, E. Hossain, and S. Camorlinga, "IEEE 802.15.4 MAC with GTS transmission for heterogeneous devices with Application to wheelchair body-area sensor networks," *IEEE Trans. Inf. Technol. in Biomedicine*, vol. 15, no. 5, pp. 767–77, Sep. 2011.
- [15] J. G. Andrews, F. Baccelli, and R. K. Ganti, "A tractable approach to coverage and rate in cellular networks," *IEEE Trans. Commun.*, vol. 59, no. 11, pp. 3122–3134, Nov. 2011.
- [16] M. Haenggi, *Stochastic geometry for wireless networks*, Cambridge Univ. Press, 2013.
- [17] R. K. Ganti, and M. Haenggi, "Spatial and temporal correlation of the interference in ALOHA ad hoc networks," *IEEE Commun. Lett.*, vol. 13, no. 9, pp. 631–633, Oct. 2009.
- [18] S. Krishnan, and H. S. Dhillon, "Spatio-temporal interference correlation and joint coverage in cellular networks," *IEEE Trans. Wireless Commun.*, vol. 16, no. 9, pp. 5659–5672, Jun. 2017.

- [19] H. Kim, S.-W. Ko, and S.-L. Kim, "Cognitive random access for internet-of-things networks," in *Proc. IEEE VTC Spring*, Sydney, Australia, May 2017.
- [20] T. Bai, and R. W. Heath, Jr., "Coverage and rate analysis for millimeter-wave cellular networks," *IEEE Trans. Wireless Commun.*, vol. 14, no. 2, pp. 1100–1114, 2015.
- [21] J. Kim, J. Park, S. Kim, S.-L. Kim, K. W. Sung, and K. S. Kim, "Millimeter-wave interference avoidance via building-aware associations," *to appear in IEEE Access*, Available at: <https://arxiv.org/abs/1712.00540>.
- [22] K. Han, K. Huang, Y. Cui, and Y. Wu, "The connectivity of millimeter-wave networks in urban environments modeled using random lattices," *arXiv preprint arXiv:1702.03372*.
- [23] A. K. Gupta, J. G. Andrews, and R. W. Heath, Jr., "Macro diversity in cellular networks with random blockages," *arXiv preprint arXiv:1701.02044*.
- [24] J. Park, S.-L. Kim, and J. Zander, "Tractable resource management with uplink decoupled millimeter-wave overlay in ultra-dense cellular networks," *IEEE Trans. Wireless Commun.*, vol. 15, no. 6, pp. 4362–4379, Jun. 2016.
- [25] H. Elshaer, M. N. Kulkarni, F. Boccardi, J. G. Andrews, and M. Dohler, "Downlink and uplink cell association with traditional macrocells and millimeter wave small cells," *IEEE Trans. Wireless Commun.*, vol. 15, no. 9, pp. 6244–6258, Sep. 2016.
- [26] Y. Li, J. G. Andrews, F. Baccelli, T. D. Novlan, and C. Zhang, "Design and analysis of initial access in millimeter wave cellular networks," *IEEE Trans. Wireless Commun.*, vol. 16, no. 10, pp. 6409–6425, Oct. 2017.
- [27] T. S. Rappaport *et al.*, "Millimeter wave mobile communications for 5G cellular: it will work!," *IEEE Access*, vol. 1, pp. 335–349, May 2013.
- [28] D. Stoyan, W. S. Kendall, and J. Mecke, *Stochastic geometry and its applications*, Wiley, 2nd edition, 1995.
- [29] M. S. Alouini, and A. J. Goldsmith, "Area spectral efficiency of cellular mobile radio systems," *IEEE Trans. Veh. Technol.*, vol. 48, no. 4, pp. 1047–1066, Jul. 1999.
- [30] A. I. Sulyman, A. T. Nassar, M. K. Samimi, G. R. MacCartney Jr., T. S. Rapaport, and A. Alsanie, "Radio propagation path loss models for 5G cellular networks in the 28 GHz and 38 GHz millimeter-wave bands," *IEEE Commun. Mag.*, vol. 52, no. 9, pp. 78–86, Sep. 2014.
- [31] S. Srinivasa, and M. Haenggi, "Path loss exponent estimation in large wireless networks," *IEEE Information Theory and Applications Workshop*, Feb. 2009.
- [32] G. Mao, B. D. O. Anderson, and B. Fidan, "Path loss exponent estimation for wireless sensor network localization," *Computer Networks*, vol. 51, no. 10, pp. 2467–2483, 2007.
- [33] X. Zhang and J. G. Andrews, "Downlink cellular network analysis with multi-slope path loss models," *IEEE Trans. Commun.*, vol. 63, no. 5, pp. 1881–1894, May 2015.
- [34] K. R. Schaubach, N. J. Davis, and T. S. Rappaport, "A ray tracing method for predicting path loss and delay spread in microcellular environments," in *Proc. IEEE VTC*, Denver, CO, USA, May 1992.
- [35] Netmanias, "LTE in Korea 2013," available at: <http://www.netmanias.com/ko/post/reports/6099/lte/lte-in-korea-2013>
- [36] E. Onur, D. Yunus, and N. Ignas, "Cooperative density estimation in random wireless ad hoc networks," *IEEE Commun. Lett.*, vol. 16, no. 3, pp. 331–333, Mar. 2012.
- [37] S. Lee and S.-L. Kim, "Optimization of time-domain spectrum sensing for cognitive radio systems," *IEEE Trans. Veh. Technol.*, vol. 60, no. 4, pp. 1937–1943, May 2011.